Nanoscale

ARTICLE

Quantitative prediction of position and orientation for an octahedral nanoparticle at liquid/liquid interfaces

Received 00th January 20xx,
Accepted 00th January 20xx

DOI: 10.1039/x0xx00000x

www.rsc.org/

Wenxiong Shi,[a] Yih Hong Lee,[b] Xing Yi Ling[b]† Shuzhou Li[a]†

Shape-controlled polyhedral particles and their assembled structures have important applications in plasmonics and biosensing, but the interfacial configurations that will critically determine their resultant assembled structures are not well-understood. Hence, a reliable theory is desirable to predict the position and orientation of a polyhedron at the vicinity of a liquid/liquid interface. Here we demonstrate that the free energy change theory can quantitatively predict the position and orientation of an isolated octahedral nanoparticle at a liquid/liquid interface, whose vertices and facets can play crucial roles in biosensing. We focus on two limiting orientations of an octahedral nanoparticle, vertex up and facet up. Our proposed theory indicates that the surface wettability (hydrophilic/hydrophobic ratio) of the nanoparticle determines its most stable position and the preferred orientation at a water/oil interface. The surface wettability of an octahedron is adjusted from extremely hydrophobic to extremely hydrophilic by changing the charge amount on the Ag surface in molecular dynamics (MD) simulations. The MD simulations results are in excellent agreement with our theoretical prediction for an Ag octahedral nanoparticle at a hexane/water interface. Our proposed theory bridges the gap between molecular-level simulations and equilibrium configurations of polyhedral nanoparticles in experiments, where insights from nanoparticles intrinsic wettability details can be used to predict macroscopic superlattice formation experimentally. This work advances our ability to precisely predict the final structures of the polyhedral nanoparticle assemblies at a liquid/liquid interface.

Introduction

The ability to predict the equilibrium assembled structure in the self-assembly of shape-controlled nanoparticle has been widely studied.[1-10] Large-area two-dimensional (2D) superlattices, which have unique nanoscale light-matter interactions, are emerging platforms with applications in all-absorptive surfaces, super resolution imaging, and smart transformation optical devices.[11-14] Interfacial assembly at a liquid/liquid interface is a powerful tool to obtain various 2D superlattices with distinct structure-dependent properties, which has been applied to nanoparticles with various shapes.[15-25] Common shape-controlled nanoparticles include polyhedron and the solids of revolution, where the latter is obtained by rotating a plane curve around an axis and includes sphere, ellipsoids, nanorods, and nanodiscs, etc.[26-29] The equilibrium position of solids of revolution at a liquid/liquid interface can be successfully obtained using free energy change theory.[30-44] However, it remains challenging for polyhedral nanoparticles to use their fundamental properties to predict their stable 2D superlattice structures at liquid/liquid interfaces, because of the complex nanoparticle-nanoparticle and nanoparticle-liquid interfacial interactions.[45, 46] The positions and orientations of polyhedral nanoparticles at the interface play key roles in determining their resultant 2D superlattices.[47-50] When the interaction between nanoparticles is weak, the position and orientation of nanoparticles at the liquid-liquid interface are determined by the fundamental properties such as geometry and hydrophilic/hydrophobic ratio.[50, 51] Since the polyhedral nanoparticles' facets and vertices in assembled superlattices with special structure can play crucial roles in polyhedral nanoparticle assembly at an interface,[52, 53] a reliable theory is needed to predict the positions and orientations of polyhedral nanoparticles at an interface.

Compared to solids of revolution, a polyhedral nanoparticle exhibits distinct anisotropic properties along different crystallographic directions.[54] The large curvatures along its tips and edges cause deep subwavelength confinement of electromagnetic fields.[23-25, 55] The polyhedral nanoparticle also has various orientations, which in turn affect the nanoscale light-matter interactions. It has been demonstrated that systematically tuning the surface wettability of a silver octahedron leads to different orientations of the octahedron, either facet up or vertex up. These orientation changes finally lead to a continuous superlattice structural evolution, from hexagonal close packing to open square structures.[47] Moreover, the interfacial behaviors of Ag nanocubes have been manipulated by controlling the hydrophilic/hydrophobic ratio conferred by capping agents, and three unique crystals have been obtained, including square close-packed, linear, and

[a] Center for Programmable Materials, School of Materials Science and Engineering, Nanyang Technological University, Singapore 639798.
[b] Division of Chemistry and Biological Chemistry, School of Physical and Mathematical Sciences, Nanyang Technological University, Singapore 637371.
† To whom correspondence should be addressed. Email: lisz@ntu.edu.sg and xyling@ntu.edu.sg.
Electronic Supplementary Information (ESI) available: [details of any supplementary information available should be included here]. See DOI: 10.1039/x0xx00000x

hexagonal lattices.[56] Therefore, to rationally design supercrystal structures from the interactions between solvents and surface capping agents of a polyhedron, the quantitative relation between these interactions and the configuration of a polyhedron need to be illustrated. It is imperative to derive a reliable method to predict the position and orientation of a polyhedron at a liquid/liquid interface, which is the basis for predicting the equilibrium structure of superlattices.

Here, we demonstrate the free energy change theory to solve the interfacial position and orientation of a polyhedral nanoparticle at a liquid/liquid interface. We use a regular octahedron as our model study due to its unique geometry. It has six vertices and eight planar facets, which can be assembled into distinct superlattices. We derive the quantitative dependence of interfacial free energy on different positions and orientations under a full range of wettability (from extremely hydrophobic to extremely hydrophilic) for an octahedron at the liquid/liquid interfaces. Our method can predict the most stable position and preferred orientation in the two limiting orientations of an octahedron when surface interactions are dominant. Molecular dynamics (MD) simulations are also performed for a silver octahedron at the hexane/water interfaces to verify our proposed theory. We tune the surface wettability (hydrophilic/hydrophobic ratio) of Ag octahedron by manipulating the amount of point charges on the surface Ag atoms while keeping the whole octahedron at charge neutral. The most stable position and preferred orientation from MD simulations are in good agreement with our extended free energy change theory. Our theory bridges the gap between molecular-level interaction simulations and nanoparticle configuration experiments, where insights from nanoparticle surface wettability can be used to predict macroscopic superlattice formation experimentally. Our findings is a step forward in predicting the equilibrium structures of polyhedral nanoparticle superlattice at a liquid/liquid interface.

Results and discussion

Configuration of an Octahedron at an oil/water Interface

The configuration of an octahedron at an oil/water interface can be described by its orientation and its position, which may determine the equilibrium structure of 2D superlattice. Many orientations can exist for an octahedron at an oil/water interface. We focus on the two extreme cases, vertex up and facet up orientation, which are mostly observed in experiments.[47] In Figure 1, the oil/water interface is set as the xy plane (not shown) and the unit vector $\hat{z}$ is pointing up along *z* direction. The octahedron has the edge length of *a*. For the vertex up orientation in the left side of Figure 1, the total height is the distance between the two opposite vertices along the z direction. H_V is the half height of octahedral nanoparticle with vertex up orientation, and $H_V = \sqrt{2}a/2$. For the facet up orientation in the right side of Figure 1, the total height is the distance between the top facet and the bottom facet along the z direction, where both facets are parallel to the interface. H_F is the half height of octahedral nanoparticle with facet up orientation, and $H_F = \sqrt{6}a/6$. The position of an octahedron is characterized by the vector from its center of mass to the oil/water interface, which is denoted as $h\hat{z}$ for both orientations, where h is negative (positive) when the most part of octahedron is in oil (water) phase. The height ratio v is defined as $v = h_V/H_V$ and $v = h_F/H_V$ for vertex up and facet up orientations, where the ranges of possible values for v are $-1 \le v \le 1$ and $-1/\sqrt{3} \le v \le 1/\sqrt{3}$, respectively (Supporting Section S3).

Free Energy Changes of an Octahedron at an oil/water Interface

According to Pieranski's free energy change theory,[28] the free energy change of a nanoparticle at an interface with height h, $F_{int}(h)$, can be rewritten with the free energy ($F(h)$) references to the free energy of the nanoparticle immersed in oil phases (F_0) for a spherical particle:

$$F_{int}(h) = F(h) - F_0 = (\gamma_{pw} - \gamma_{po})A_{pw} - \gamma_{wo}A_{st} + \tau L \quad (1)$$

where γ_{pw}, γ_{po}, γ_{wo} and τ are the particle/water, particle/oil, oil/water surface tensions, and the three-phase line tension, respectively. A_{pw}, A_{st}, and L are the particle/water interface area, oil/water interface area occupied by the nanoparticle, and the length of three-phase line, respectively. For a given system, the values of all surface tensions and the line tension are independent of the configuration of the octahedron while only A_{pw}, A_{st}, and L are functions of the configuration of the octahedron. Equation (1) has been applied to predict the equilibrium height of a sphere, as shown in Supporting Section S1, and to investigate nanoparticles of different shapes, such as pillars, ellipsoids, and even Janus type nanoparticles.[39, 40, 57, 58] Furthermore, the contribution of the line tension is ignored since it is one order of magnitude lower than surface tension.[29] When the line tension is ignored, the free energy change in equation (1) becomes

$$F_{int}(h) = F(h) - F_0 = (\gamma_{pw} - \gamma_{po})A_{pw} - \gamma_{wo}A_{st} \quad (2)$$

Divided by $A\gamma_{wo}$ on both sides to get the unit less formula, the equation (2) becomes

$$F = F_{int}(h)/(A\gamma_{wo}) = RA_{pw}/A - A_{st}/A, \quad \text{where } R = (\gamma_{pw} - \gamma_{po})/\gamma_{wo}. \quad (3)$$

F is the $F_{int}(h)$ normalized by octahedron surface area *A* and oil/water surface tension γ_{wo}. R is the surface tension ratio, and has the opposite sign compared to cosine contact angle, where $\cos\theta = (\gamma_{po} - \gamma_{pw})/\gamma_{wo}$. This means R is positive (negative) when the most part of octahedron is in oil (water) phase, which means the surface of octahedron is hydrophobic (hydrophilic). In this formula, the surface tensions are determined by the interactions between the octahedron and solvents. Moreover, the particle/water contact surface area A_{wp}, and oil/water cross contact surface area A_{st} depend on the positions and orientations of the octahedron on the oil/water interface with two limiting orientations. Therefore, the formulas are derived to calculate the A_{wp}, and A_{st} for these two limiting orientations, which are shown below.

(a) Vertex up orientation:

As defined before, the half-height in vertex up orientation $H_V = \sqrt{2}a/2$, where *a* is the edge length of an octahedron. With the total surface area $A = 2\sqrt{3}a^2$ and the height ratio $v = h_V/H_V$,

the particle/water interface area A_{pw} can be calculated from equation (4) for an octahedron with vertex up orientation.

$$A_{pw} = \begin{cases} A \times \frac{(1-|v|)^2}{2} & -1 \le v \le 0 \\ A - A \times \frac{(1-|v|)^2}{2} & 0 < v \le 1 \end{cases} \quad (4)$$

The oil/water interface area occupied by the octahedron A_{st} can be calculated from equation (5):

$$A_{st} = a^2 \times (1-|v|)^2 \quad (5)$$

Since the express of A_{pw} depends on the sign of v, we discuss equation (3) in two regions: $-1 \le v \le 0$ and $0 < v \le 1$, which means the octahedron is immersed into oil phase and water phase, respectively.

$$F = \begin{cases} \left(\frac{R}{2} - \frac{1}{2\sqrt{3}}\right)(v^2 + 2v + 1) & -1 \le v \le 0, \ a \\ -\left(\frac{1}{2\sqrt{3}} + \frac{R}{2}\right)(v^2 - 2v + 1) & 0 < v \le 1, \ b \end{cases} \quad (6)$$

The minimum value of F depends on the location of the axis of symmetry p and the orientation of the parabola. a_1, b_1 and a_2, b_2 are the coefficients for the equation (6)a and b, respectively, as shown in Supporting Section S3. Based on the location of p and the orientation of the parabola, we can divide the region -1~1 to five regions, which are (1) $-1 \le R < -\sqrt{3}/3$, (2) $R = -\sqrt{3}/3$, (3) $-\sqrt{3}/3 < R < \sqrt{3}/3$, (4) $R = \sqrt{3}/3$, and (5) $\sqrt{3}/3 < R \le 1$, as shown in Figure 2a and Table 1.

(1) In the case of $-1 \le R < -\sqrt{3}/3$.

As discussed in Supporting Section S3c, when $v = 1$, F reaches its minimum value of R, the octahedron is more hydrophilic and prefers to stay in water. F is plotted as the function of v in Figure 2b curve 1, where *R* = – 0.7.

(2) In the case of $R = -\sqrt{3}/3$.

Similarly, F reaches its minimum value of R in the region of $0 < v \le 1$, which means that the octahedron prefers to stay in water with any position. F is plotted as a function of v in Figure 2b curve 2, where *R*=$-\sqrt{3}/3$. As discussed in Supporting Section S3, the relationship between *R* and v is that *R* is a constant with $R = \sqrt{3}/3 = (\gamma_{pw} - \gamma_{po})/\gamma_{wo}$. v is canceled in the analysis and the *R* does not depend on v, arising from the planar surface of the octahedron. Based on the contact angle definition and mathematical calculation, the four facets of an octahedron in water have identical contact angles in the region of $0 < v \le 1$, which is $\sqrt{3}/3$. Therefore, the octahedron prefers to stay in water with any position when *R* =$-\sqrt{3}/3$.

(3) In the case of $-\sqrt{3}/3 < R < \sqrt{3}/3$.

When $v = 0$, F reaches its minimum value of $(3\mathrm{R} - \sqrt{3})/6$, half octahedron stays in water and half octahedron stays in oil. The F has its maximum value of 0 at $v = -1$, when *R* is negative, while it has its maximum value of R at $v = 1$ when *R* is positive. F is plotted in Figure 2b curve 3, where R = – 0.2.

(4) In the case of $R = \sqrt{3}/3$.

In the region of $-1 \le v \le 0$, F reaches its minimum value of 0, which means that octahedron prefers to stay in oil with any position. F is plotted in Figure 2b curve 4, where R = $\sqrt{3}/3$.

(5) In the case of $\sqrt{3}/3 < R \le 1$.

When $v = -1$, F reaches its minimum value of 0, which means that octahedron is more hydrophobic and prefers to stay in oil. F is plotted in Figure 2b curve 5, where R = 0.7.

(b) Facet up orientation:

In a facet up orientation, the total height is the distance between the top facet and the bottom facet along the z direction, where both surfaces are parallel to the interface. Therefore, the half-height $H_F = \sqrt{6}a/6$, and $f = h_F/H_F$. With $H_V = \sqrt{2}a/2$, the f and v is different by a factor $\sqrt{3}$, which is $f = \sqrt{3}v$.

Because $-1 \le f \le 1$, the range of height ratio is $-\sqrt{3}/3 \le v \le \sqrt{3}/3$.

As shown in supporting Figure S1 and Figure S2 in Supporting Section S2, we can get the particle/water contact surface area A_{wp}, and oil/water cross contact surface area A_{st} for the facet up orientation.

$$A_{wp} = \frac{1}{8}A + \frac{3}{4}A \times \frac{1+f}{2} \quad (7)$$

$$A_{st} = \frac{1}{8}A \times \left(\left(\frac{3+f}{2}\right)^2 - 3\left(\frac{1+f}{2}\right)^2\right) \quad (8)$$

For the free energy change, the main equation for facet up orientation is

$$F = \frac{1}{16}f^2 + \frac{3R}{8}f + \frac{8R-3}{16}, \ -1 \le f \le 1, \quad (9)$$

To compare the results in vertex up orientation, we substitute $f = \sqrt{3}v$ into the equation (9), which becomes

$$F = \frac{3}{16}v^2 + \frac{3\sqrt{3}R}{8}v + \frac{8R-3}{16}, \ -\sqrt{3}/3 \le v \le \sqrt{3}/3 \quad (10)$$

where the region of *R* is $-1 \le R \le 1$.

From $-1 \le R \le 1$ and $p = -\sqrt{3}R$, the range of the axis of symmetry p could be $-\sqrt{3} \le p \le \sqrt{3}$. However, the range of v is only $-\sqrt{3}/3 \le v \le \sqrt{3}/3$ for facet up orientation. We will discuss the dependence of F on v in three regions:$-1 \le R < -1/3$, $-1/3 \le R \le 1/3$, and $1/3 < R \le 1$, where $p > \sqrt{3}/3$, $-\sqrt{3}/3 \le p \le -\sqrt{3}/3$, and $p < -\sqrt{3}/3$, as shown in Figure 3a and Table 2.

(1) In the case of $-1 \le R < -1/3$, F is monotonic decreasing with v in the whole range since the axis of symmetry p is larger or equals to $\sqrt{3}/3$. Therefore, F reaches its minimum value of $(7R-1)/8$ when $v = \sqrt{3}/3$ and the octahedron prefers to stay in water, which is illustrated in Figure 3b curve 1 with R = – 0.5.

(2) In the case of $-1/3 \le R \le 1/3$, the axis of symmetry p falls into the allowed range of v and the parabola opens upward. Therefore, F reaches its minimum value of $(-9R^2 + 8R - 3)/16$ when $v = -\sqrt{3}R$, which means that the position of octahedron changes with R, which is illustrated in Figure 3b curve 2 with R = – 0.2.

(3) In the case of $1 < R \le \sqrt{3}/3$, F is monotonic increasing with v in the whole range since the axis of symmetry p is smaller or equal to $-\sqrt{3}/3$. Therefore, F reaches its minimum value of $(R-1)/8$ when $v = -\sqrt{3}/3$ and the octahedron prefers to stay in oil, which is illustrated in Figure 3b curve 3 with R = 0.5.

(c) The most stable region for octahedron with the facet up and vertex orientation.

For vertex up orientation, the minimum value of F are *R*, $(3\mathrm{R} - \sqrt{3})/6$, and 0 for the regions $-1 \le R < -\sqrt{3}/3$, $-\sqrt{3}/3 < R < \sqrt{3}/3$, and $-\sqrt{3}/3 < R \le 1$, respectively. The cases of $R = (\gamma_{pw} - \gamma_{po})/\gamma_{wo} = \pm\sqrt{3}/3$ are special points, where the octahedron can stay in water or oil phase with vertex up at any positions. However, surface tension γ_{pw} and γ_{po} should have a

specific value compared to γ_{wo}, which is difficult to achieve in experiment, so that the two special points would not be discussed further. For facet up orientation, the minimum value of F are $(7R-1)/8$, $(-9R^2+8R-3)/16$, and $(R-1)/8$ for the regions: $-1 \le R < -1/3$, $-1/3 \le R \le 1/3$, and $1/3 < R \le 1$, respectively. All these results are summarized in Table 3 and plotted in Figure 4. The free energy change minimum F are shown and compared in Figure 4 for both orientations. When $-1 \le R < (3-4\sqrt{3})/9$ or $(4\sqrt{3}-3)/9 < R \le 1$, the minimum of free energy change in facet up orientation is smaller than that in vertex up orientation, thus the octahedron favors facet up orientation. When $(3-4\sqrt{3})/9 \le R \le (4\sqrt{3}-3)/9$, the minimum of free energy change in facet up orientation is larger than that in vertex up orientation, thus the octahedron favors vertex up orientation.

Position and Orientation of an Octahedral Nanoparticle System in MD Simulation.

The quantitative dependence of interfacial free energy on different positions and orientations under a full range of wettability for an octahedron at liquid/liquid interfaces are derived for two limiting orientations, vertex up and facet up. The orientations and positions of an octahedron at the oil/water interface under different wettability can be obtained from MD simulations. We build a model system which is comparable to the experimental condition, enabling us to derive molecular-level insights on the interfacial behaviors. To verify our extended free energy change theory for an octahedral nanoparticle at a liquid/liquid interface, MD simulations are performed using an octahedral silver nanoparticle on a hexane/water interface. In our MD simulations, the Ag octahedron is built using 344 Ag atoms inside as the core and 326 surface Ag atoms outside as the surface layer. The surface wettability of Ag octahedron is adjusted by changing the charge amount (q) on the surface Ag atoms, where the unit is elementary charge (e) as depicted in Supporting Section S4 and shown in Figure S4. The positive or negative partial charge are randomly introduced on 326 outside Ag atoms, and the total net charge is zero for Ag octahedron.[59, 60] Therefore, the Ag octahedron is still an electrically neutral particle, and does not carry any extra charge for the simulation system. The size of octahedron is about 3 nm in our MD simulations, where the gravity force can be ignored.[49] The Ag octahedron is put into the vicinity of hexane/water interface, and the position and orientation are evolved as the function of time for various *q*. Five typical equilibrium position and orientation of the silver octahedron are shown in Figure 5a for *q* = 0.1 e, 0.13 e, 0.18 e, 0.45 e and 0.49 e, respectively. Surface wettability increases with *q* increases, which can be quantified by surface tension ratio *R*, as discussed in below. Increasing *q* enhances the hydrophilicity of the octahedron surface, which favors stronger interaction with the polar solvent, water. As shown in Figure 5a, the octahedron breaches the hexane/water interface. The equilibrium position of silver octahedron moves from oil phase (0.1 e ~ 0.18 e) to water phase (0.18 e ~ 0.49 e), with accompanying orientation change, as the wettability increases. Its position and orientation is governed by the competition between the octahedron-water (NP-Water) and octahedron-hexane (NP-Hexane) interactions, which is defined as the hydrophilic/hydrophobic interaction energy. As *q* increases, the interaction energy between the octahedron and water also increase, as shown in Figure 5b. Water is a polar solvent, and has strong electrostatic interaction with octahedron with high *q*. Thus, a larger part of the octahedron immerses into water. Conversely, the interaction energy between the octahedron and hexane decreases, leading to octahedron moving away from hexane. Therefore, if the octahedron with desired wettability can be obtained by choosing proper ligands, targeted superlattices be fabricated by using these octahedra.

The Calculation of Height Ratio v in MD Simulation.

The analytical method only focus on two limiting orientations, vertex up and facet up. For MD simulation, due to the thermodynamic fluctuation and lack of constraint for the two orientations, it is reasonable for the octahedral nanoparticle to exhibit various tilt orientations, but most of these orientations are close to the two limiting orientations. Therefore, the height ratio v in MD simulation can be obtained after treatment by $v = h_V/H_V$ and $v = h_F/H_V$ for vertex up and facet up orientations, respectively. h_V, h_F, H_V and H_F are obtained from positions of silver octahedron, position of center of silver octahedron and position of oil/water interface. The equilibrium positions of the silver octahedron are extracted from the density profiles of the three components (Ag, water, and hexane) along the vertical direction of the simulation box for octahedrons with different value of *q*, as shown in supporting Figure S7, where only water and hexane density in *q* = 0.1 e system are shown for clarity. In this figure, the interfacial positions of hexane/water for all the systems are moved to same position. To track the geometric center of Ag octahedron in a simulation trajectory, the geometric center of octahedron is averaged through 100 ps period. Because the octahedron shows a lot of tilt orientations in MD simulations, the total octahedron height is calculated as the distance from the starting point to the ending point of Ag density distribution profile in MD simulations. Therefore, the value of H_V is the half of the total octahedron height when the octahedron is close to a vertex up orientation. For facet up orientations, the half-height equals the value of H_F. Because the thickness of hexane/water interface is about 0.3-0.5 nm in our simulations, which is caused by the interface deformation and the large interface region, the value of h_V or h_F depends on the relative position of octahedron to the position of oil/water interface. When a vertex (a facet) of the octahedron in one phase just starts to contact or enter the other phase, as shown in 0.10 e in Figure 5a and Figure 5c (0.13 e in Figure 5a and Figure 5d), the position of interface is defined as the starting point of density curve of the other phase near the surface. When the octahedron has significant proportions in both liquid phases, as shown in Figure 5e, the position of interface is defined as the middle line of two solvent density curves near the surface, so the value of h_V or h_F in simulations is the distance between the geometric center of Ag octahedron and the interface, which is shown in supporting information. Therefore, we can get height ratio $v = h_V/H_V$. The value of v equals −0.890 for octahedron with *q* = 0.1 e, where most of octahedron is immersed into the oil phase as shown in Figure 5d. The values of v are listed in Table 4 for an octahedron with other amount of charges.

The Calculation of Surface Tension Ratio R in MD Simulation.

The surface tensions between Ag slabs and solvents can be obtained using MD simulations, as shown in Figure.S5 in supporting information S5. The interfacial tensions γ is defined as the difference of the normal pressure (P_N) and lateral pressure (P_L) in the box:

$$\gamma = < (P_N - P_L) L_Z > /2 \quad (11)$$

where L_z is the box size along the normal direction and $P_L=(P_{xx}+P_{yy})/2$, where P_{xx} and P_{yy} are pressure along the xx and yy directions. The factor (1/2) outside the bracket takes into account the fact that there are two interfaces in the system.[61-63] The surface tension between water and oil is also calculated with the same method. The value of *R* can be calculated from $R = (\gamma_{pw} - \gamma_{po})/\gamma_{wo}$.

Only when the value of *q* is small, our charged Ag octahedron model can have reliable free energy change at an oil/water interface. When the value of *q* is large, where more than a half of the octahedron is immersed into water phase, the water molecules near the Ag surface are polarized by electric fields and stick on the Ag surface due to the strong water-Ag electrostatic attraction,[64-66] as shown in supporting Figure S6. This artificial cage effect blocks the access of oil molecules to the Ag surface. Since the interfacial behavior in $-1 \le R < 0$ is the mirroring behavior as in the region of $0 \le R \le 1$, we only discuss the region of $0 \le R \le 1$ in the following discussion.[40]

The Equilibrium Orientation from MD Simulations and Analytical Method.

The orientation of octahedron at hexane/water interface with different wettabliity can be easily extracted from MD simulation. The free energy change of the Ag octahedron adsorbed at an oil/water interfacial system can be calculated from the surface tension and interfacial area, which is shown in Equation (3). The free energy change is normalized by $A\gamma_{wo}$, which equals 348.7 k_BT in our simulation systems, where the octahedron length is about 3 nm. Based on the reference energy $A\gamma_{wo}$, the increase length size by 1 order of magnitude would enhance the surface area change by 2 order of magnitude, and then enhance the free energy change by 2 order of magnitude. As shown in Figure 6, the free energy changes for two standard orientations, vertex up and facet up, were plotted as the function of the height ratio in oil phase. For *q* = 0.18 e where *R* has a value of 0.135 ± 0.043, the free energy change curves calculated from equation 5, 6 and equation 10 are plotted in Figure 6(a1) for the vertex up orientation and the facet up orientation, respectively. The three snapshots from MD simulations are shown in Figure 6(a2-a4). The octahedron shows vertex up orientations in MD simulations as predicted by free energy change theory, even though all vertex up orientations are tilted. The free energy change difference for the two orientations is about 34.87 k_BT, which is higher than the thermodynamic fluctuation, several k_BT. For the octahedral Ag nanoparticle with about 300 nm length in experiment, the free energy change difference for the two orientations is about 3.5×10^5 k_BT. The huge free energy difference would be the driving force to form lower energy structure superlattices. For *q* = 0.13 e where *R* has a value of 0.547 ± 0.021, the free energy change curves calculated from equations 5, 6 and 10 are plotted in Figure 6(b1) for the vertex up orientation and the facet up orientation, respectively. From our extended free energy change theory, the octahedron should have facet up orientation at equilibrium configuration. The three snapshots from MD simulations are shown in Figure 6(b2-b4). It's obvious that the octahedron is in facet up orientation, which is in excellent agreement with our theoretical prediction. For the octahedron with *q* = 0.1 e where *R* has a value of 0.810 ± 0.037, the octahedron is more hydrophobic and should have facet up orientation from the energy analysis, which is shown in Figure 4. The free energy change curve calculated from equations 5 and 6 is plotted for the vertex up and facet up orientation in Figure 6(c1). In the value of $R = 0.810 \pm 0.037$, the difference between the energy change curve for two orientations is very small. Moreover, the three snapshots from MD simulations illustrated that the octahedron is in vertex up orientation, which is immersed in oil phase with a tip into the water phase, as shown in Figure 6(c2-c4). This mismatch is caused by the neglect of the contribution of the line tension in our free energy difference theory. The length of three-phase line *L* for vertex up and facet up orientations are about 0 nm, and 9 nm, respectively, as shown in supporting Figure S3. The line tension, which obstruct the particle cross the water/oil interface, would apply the negative effect for the facet up orientation, which has long length of three-phase line. Therefore, for the regions of R with small energy difference for two orientations, the orientation can be affected by line tension and favors over the vertex up orientation. The interfacial evolution in water phase should be the mirroring behavior in oil phase.[40]

The Equilibrium Position from MD and Analytical Method.

The position of octahedron at hexane/water interface with different wettabliity can be easily extracted by MD simulation. After the octahedron reaches its equilibrium position, the value of height ratio v is extracted and is averaged through 100ps. The height ratio v and surface tension ratio *R* from MD simulations are also shown in Figure 7. Our previous extended free energy change results are summarized in Table 3: the octahedron favors half in water and half in oil with $v = 0$ when $0 \le R \le (4\sqrt{3} - 3)/9$; it stays on the oil/water interface with one facet contacting with water with $h_e \approx -\sqrt{3}/3$ when $(4\sqrt{3} - 3)/9 < R \le 1$; it immerses in oil with $v = -1$ when $R = 0.810$. These results are plotted in the Figure 7, where the green, red, blue lines represent $h_e = 0$, and $h_e = -\sqrt{3}/3$, respectively. The MD results show good agreement with analytical results even though only two limiting orientations are considered in our analysis. In the range of $(3 - 4\sqrt{3})/9 \le R \le (4\sqrt{3} - 3)/9$, the value of h_e is around 0. We extend the range of *R* from $0 \le R \le (4\sqrt{3} - 3)/9$ to $(3 - 4\sqrt{3})/9 \le R \le (4\sqrt{3} - 3)/9$, because the octahedron with R in this range has same equilibrium position and vertex orientation. In the range of $(4\sqrt{3} - 3)/9 < R \le 1$, the value of h_e fluctuates around $-\sqrt{3}/3$. For the points of R close to 1, the orientation can be affected by line tension and favors over the vertex up orientation with $h_e = -1$. The magnitude of fluctuations is relative large for v from MD simulations. It may be due to the fact that the octahedron has a lot of tilt orientations, especially when it has one vertex pointing up. It is very rare for an

octahedron to have the straight vertical up orientation in MD simulations. The tilt orientations affect the free energy change and introduce the fluctuation of height ratio v. Therefore, the agreement between MD simulation results and extended free energy change theory could be improved if the tilt orientations and line tension were considered in the extended free energy change theory. Moreover, since our octahedron length is about 3 nm, the difference of two limiting orientation is about 34.87 k_BT, which is about is one order of magnitude higher than the thermodynamic fluctuation. As the size of octahedron increases, such as the experimental Ag octahedron with around hundreds of nanometers, the huge free energy difference would precisely predict the position and orientation of the octahedron. Using our extended free energy change theory, once the ligands were chosen, the nanoparticles' wettability was settled, then, the orientation and its position of the octahedron at an oil/water interface can be determined, which would determine the equilibrium structure of 2D superlattices, especially when surface interactions are dominant. Once the position and orientation are settled, the nanoparticles can be guided to assemble into desired structures. Moreover, based on our desired superlattices' structure, which is vertex up or facet up, the proper wettability can be settled, and then, the suitable ligands can be chosen as the building block to self-assemble into our desired superlattices.

Conclusions

We demonstrate the free energy change theory to an isolated octahedral nanoparticle at a liquid/liquid interface. Our results demonstrate the relationship between the surface tension and interfacial geometry, which can determine interfacial properties, such as position and orientation. Therefore, the equilibrium configuration of an octahedron can be predicted by our simple free energy change theory. The position and orientation of an octahedron at oil/water interfaces are determined by the surface tensions, γ_{pw}, γ_{po}, and γ_{wo}. With the decreasing of the particle-water surface tension γ_{pw}, the preferred orientation of an octahedron changes from vertex up (caused by line tension) to facet up, and then vertex up, with the position change accordingly. In our MD simulations, the surface wettability of Ag octahedral nanoparticle is modified by the charge amount on surface Ag atoms while the whole octahedron is kept at charge neutral. Increasing the wettability of Ag octahedron surface leads to the translocation from oil phase into water phase with various orientation. The position and orientation of octahedral nanoparticle in the vicinity of interface play a key role in the process of self-assembly, especially for the polyhedral nanoparticles. The stable configurations in molecular dynamics simulations are in excellent agreement with the results from our theoretical prediction. This theory may move a step forward to precisely predict the equilibrium structures of the polyhedral nanoparticle assemblies at a liquid/liquid interface.

Acknowledgements

We thank the support from Academic Research Fund Tier 1 (RG107/15). X.Y.L. and Y. H. L. thank the financial support from National Research Foundation, Singapore (NRF-NRFF2012-04) and Nanyang Technological University's start-up grant.

Notes and references

1. G. M. Whitesides and B. Grzybowski, *Science*, 2002, **295**, 2418-2421.
2. P. F. Damasceno, M. Engel and S. C. Glotzer, *Science*, 2012, **337**, 453-457.
3. C. J. Zeng, Y. X. Chen, K. Kirschbaum, K. J. Lambright and R. C. Jin, *Science*, 2016, **354**, 1580-1584.
4. H. Mundoor, B. Senyuk and Smalyukh, II, *Science*, 2016, **352**, 69-73.
5. V. N. Manoharan, *Science*, 2015, **349**, 8.
6. M. J. Huang, C. H. Hsu, J. Wang, S. Mei, X. H. Dong, Y. W. Li, M. X. Li, H. Liu, W. Zhang, T. Z. Aida, W. B. Zhang, K. Yue and S. Z. D. Cheng, *Science*, 2015, **348**, 424-428.
7. T. Dotera, T. Oshiro and P. Ziherl, *Nature*, 2014, **506**, 208-211.
8. E. Bianchi, C. N. Likos and G. Kahl, *ACS Nano*, 2013, **7**, 4657-4667.
9. J. de Graaf and L. Manna, *Science*, 2012, **337**, 417-418.
10. J. Henzie, M. Gruenwald, A. Widmer-Cooper, P. L. Geissler and P. Yang, *Nat. Mater.*, 2012, **11**, 131-137.
11. J. M. Hao, J. Wang, X. L. Liu, W. J. Padilla, L. Zhou and M. Qiu, *Appl. Phys. Lett.*, 2010, **96**, 3.
12. M. Hentschel, M. Saliba, R. Vogelgesang, H. Giessen, A. P. Alivisatos and N. Liu, *Nano Lett.*, 2010, **10**, 2721-2726.
13. S. Zhang, W. J. Fan, N. C. Panoiu, K. J. Malloy, R. M. Osgood and S. R. J. Brueck, *Phys. Rev. Lett.*, 2005, **95**, 4.
14. D. Shin, Y. Urzhumov, D. Lim, K. Kim and D. R. Smith, *Sci. Rep.*, 2014, **4**, 9.
15. C. Zhang, X. Zhang, X. Zhang, X. Ou, W. Zhang, J. Jie, J. C. Chang, C.-S. Lee and S.-T. Lee, *Adv. Mater.*, 2009, **21**, 4172-4175.
16. Y. Lin, A. Böker, H. Skaff, D. Cookson, A. D. Dinsmore, T. Emrick and T. P. Russell, *Langmuir*, 2005, **21**, 191-194.
17. Y. Lin, H. Skaff, T. Emrick, A. D. Dinsmore and T. P. Russell, *Science*, 2003, **299**, 226-229.
18. A. Boker, Y. Lin, K. Chiapperini, R. Horowitz, M. Thompson, V. Carreon, T. Xu, C. Abetz, H. Skaff, A. D. Dinsmore, T. Emrick and T. P. Russell, *Nat. Mater.*, 2004, **3**, 302-306.
19. Y. Lin, H. Skaff, A. Böker, A. D. Dinsmore, T. Emrick and T. P. Russell, *J. Am. Chem. Soc.*, 2003, **125**, 12690-12691.
20. J. T. Russell, Y. Lin, A. Böker, L. Su, P. Carl, H. Zettl, J. He, K. Sill, R. Tangirala, T. Emrick, K. Littrell, P. Thiyagarajan, D. Cookson, A. Fery, Q. Wang and T. P. Russell, *Angew. Chem. Int. Edn*, 2005, **44**, 2420-2426.
21. J. A. Fan, C. Wu, K. Bao, J. Bao, R. Bardhan, N. J. Halas, V. N. Manoharan, P. Nordlander, G. Shvets and F. Capasso, *Science*, 2010, **328**, 1135-1138.
22. K. E. Mueggenburg, X.-M. Lin, R. H. Goldsmith and H. M. Jaeger, *Nat. Mater.*, 2007, **6**, 656-660.
23. Z. Nie, A. Petukhova and E. Kumacheva, *Nat. Nanotechnol.*, 2010, **5**, 15-25.
24. A. Dong, J. Chen, P. M. Vora, J. M. Kikkawa and C. B. Murray, *Nature*, 2010, **466**, 474-477.

25. A. Tao, P. Sinsermsuksakul and P. Yang, *Nat. Nanotechnol.*, 2007, **2**, 435-440.
26. S. U. Pickering, *J. Chem. Soc., Trans.*, 1907, **91**, 2001-2021.
27. W. Ramsden, *Proc. R. Soc. London, Ser. A*, 1903, **72**, 156-164.
28. P. Pieranski, *Phys. Rev. Lett.*, 1980, **45**, 569-572.
29. R. Ranatunga, R. J. B. Kalescky, C. C. Chiu and S. O. Nielsen, *J. Phys. Chem. C*, 2010, **114**, 12151-12157.
30. T. Wang, J. Zhuang, J. Lynch, O. Chen, Z. Wang, X. Wang, D. LaMontagne, H. Wu, Z. Wang and Y. C. Cao, *Science*, 2012, **338**, 358-363.
31. H. Heinz, R. A. Vaia, B. L. Farmer and R. R. Naik, *J. Phys. Chem. C*, 2008, **112**, 17281-17290.
32. X. Ye, J. Chen, M. Engel, J. A. Millan, W. Li, L. Qi, G. Xing, J. E. Collins, C. R. Kagan, J. Li, S. C. Glotzer and C. B. Murray, *Nat. Chem.*, 2013, **5**, 466-473.
33. W. Lu, Q. Liu, Z. Sun, J. He, C. Ezeolu and J. Fang, *J. Am. Chem. Soc.*, 2008, **130**, 6983-6991.
34. T. Ming, X. Kou, H. Chen, T. Wang, H.-L. Tam, K.-W. Cheah, J.-Y. Chen and J. Wang, *Angew. Chem. Int. Ed.*, 2008, **47**, 9685-9690.
35. M. P. Boneschanscher, W. H. Evers, J. J. Geuchies, T. Altantzis, B. Goris, F. T. Rabouw, S. A. P. van Rossum, H. S. J. van der Zant, L. D. A. Siebbeles, G. Van Tendeloo, I. Swart, J. Hilhorst, A. V. Petukhov, S. Bals and D. Vanmaekelbergh, *Science*, 2014, **344**, 1377-1380.
36. K. Miszta, J. de Graaf, G. Bertoni, D. Dorfs, R. Brescia, S. Marras, L. Ceseracciu, R. Cingolani, R. van Roij, M. Dijkstra and L. Manna, *Nat. Mater.*, 2011, **10**, 872-876.
37. K. L. Gurunatha, S. Marvi, G. Arya and A. R. Tao, *Nano Lett.*, 2015, **15**, 7377-7382.
38. C.-W. Liao, Y.-S. Lin, K. Chanda, Y.-F. Song and M. H. Huang, *J. Am. Chem. Soc.*, 2013, **135**, 2684-2693.
39. J. He, Q. Zhang, S. Gupta, T. Emrick, T. R. Russell and P. Thiyagarajan, *Small*, 2007, **3**, 1214-1217.
40. J. Faraudo and F. Bresme, *J. Chem. Phys.*, 2003, **118**, 6518-6528.
41. H. Rapaport, H. S. Kim, K. Kjaer, P. B. Howes, S. Cohen, J. Als-Nielsen, M. R. Ghadiri, L. Leiserowitz and M. Lahav, *J. Am. Chem. Soc.*, 1999, **121**, 1186-1191.
42. E. Dujardin, T. W. Ebbesen, A. Krishnan and M. M. J. Treacy, *Adv. Mater.*, 1998, **10**, 1472-1475.
43. E. Snoeks, A. van Blaaderen, T. van Dillen, C. M. van Kats, M. L. Brongersma and A. Polman, *Adv. Mater.*, 2000, **12**, 1511-1514.
44. F. Gunther, S. Frijters and J. Harting, *Soft Matter*, 2014, **10**, 4977-4989.
45. M. Grzelczak, J. Vermant, E. M. Furst and L. M. Liz-Marzan, *Acs Nano*, 2010, **4**, 3591-3605.
46. E. M. Furst, *Proc. Natl. Acad. Sci. U. S. A.*, 2011, **108**, 20853-20854.
47. Y. H. Lee, W. X. Shi, H. K. Lee, R. B. Jiang, I. Y. Phang, Y. Cui, L. Isa, Y. J. Yang, J. F. Wang, S. Z. Li and X. Y. Ling, *Nat. Commun.*, 2015, **6**, 6990.
48. A. Boker, J. He, T. Emrick and T. P. Russell, *Soft Matter*, 2007, **3**, 1231-1248.
49. F. Bresme and M. Oettel, *J. Phys. Condens. Matter.*, 2007, **19**, 413101.
50. Z. Huang, P. Chen, Y. Yang and L.-T. Yan, *J. Phys. Chem. Lett.*, 2016, **7**, 1966-1971.
51. H. Rezvantalab and S. Shojaei-Zadeh, *ACS Nano*, 2016, **10**, 5354-5361.
52. J. J. Geuchies, C. van Overbeek, W. H. Evers, B. Goris, A. de Backer, A. P. Gantapara, F. T. Rabouw, J. Hilhorst, J. L. Peters, O. Konovalov, A. V. Petukhov, M. Dijkstra, L. D. A. Siebbeles, S. van Aert, S. Bals and D. Vanmaekelbergh, *Nat. Mater.*, 2016, **15**, 1248-1254.
53. M. C. Weidman, D. M. Smilgies and W. A. Tisdale, *Nat. Mater.*, 2016, **15**, 775-+.
54. J. G. Donaldson and S. S. Kantorovich, *Nanoscale*, 2015, **7**, 3217-3228.
55. M. B. Ross, M. G. Blaber and G. C. Schatz, *Nat. Commun.*, 2014, **5**.
56. Y. Yang, Y. H. Lee, I. Y. Phang, R. Jiang, H. Y. F. Sim, J. Wang and X. Y. Ling, *Nano Lett.*, 2016, **16**, 3872-3878.
57. B. P. Binks and P. D. I. Fletcher, *Langmuir*, 2001, **17**, 4708-4710.
58. R. Erhardt, M. Zhang, A. Böker, H. Zettl, C. Abetz, P. Frederik, G. Krausch, V. Abetz and A. H. E. Müller, *J. Am. Chem. Soc.*, 2003, **125**, 3260-3267.
59. J. P. P. Ramalho, P. Gkeka and L. Sarkisov, *Langmuir*, 2011, **27**, 3723-3730.
60. D. Zhang, P. Gonzalez-Mozuelos and M. O. de la Cruz, *J. Phys. Chem. C*, 2010, **114**, 3754-3762.
61. Y. H. F. Zhang, S. E.; Brooks, B. R.; Pastor, R. W. , *J. Chem. Phys.*, 1995, **103**.
62. J. L. M. Rivera, C.; Cummings, P. T. , *Phys. ReV. E* 2003, **67**.
63. H. J. C. P. Berendsen, J. P. M.; Gunsteren, W. F.; Hermans, J., *Intermolecular Forces; Reidel: Dordrecht, 1981*.
64. M. Darvas, M. Jorge, M. Cordeiro and P. Jedlovszky, *J. Phys. Chem. C*, 2011, **115**, 11140-11146.
65. B. J. Newton, K. A. Brakke and D. M. A. Buzza, *Phys. Chem. Chem. Phys.*, 2014, **16**, 26051-26058.
66. B. J. Newton and D. M. A. Buzza, *Soft Matter*, 2016, **12**, 5285-5296.

Nanoscale

ARTICLE

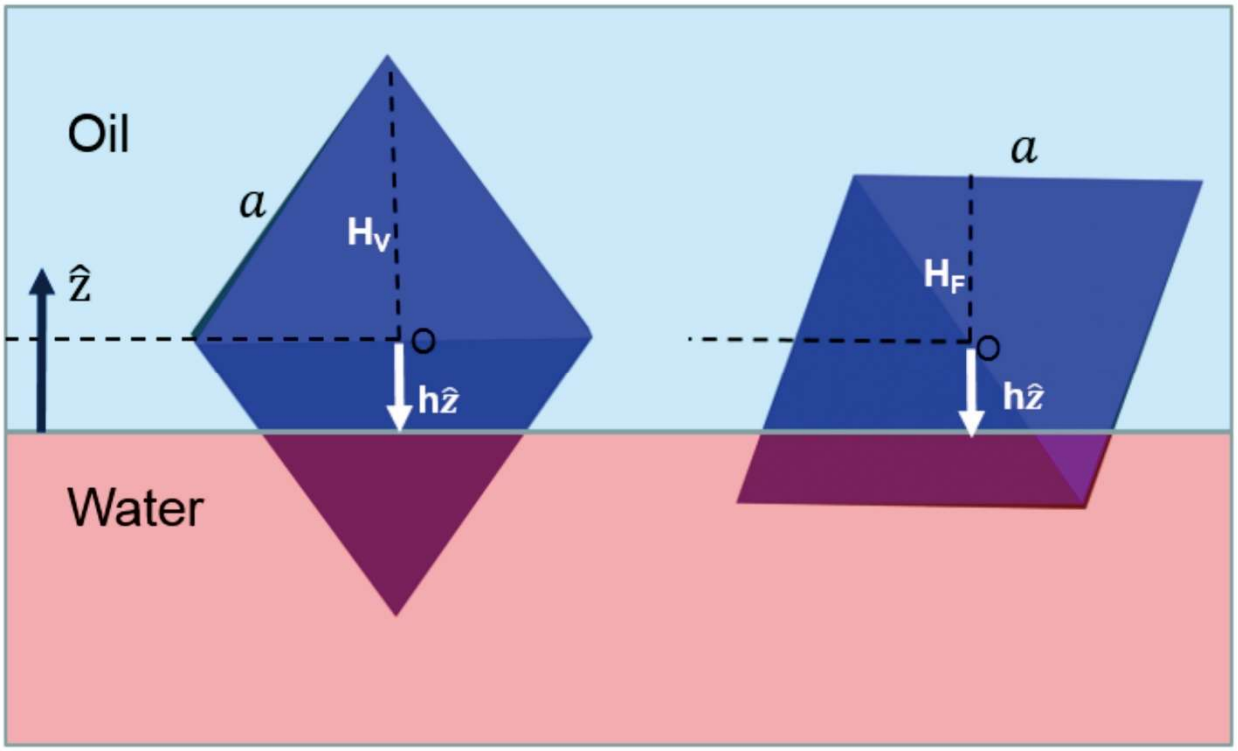

Figure 1. Sketch of an octahedral nanoparticle in the vicinity of an oil/water interface. The vertex up orientation is on the left side and the facet up orientation is on the right side. The octahedron has edge length of a. The unit vector $\hat{z}$ is pointing up along the z direction. The vector from the center of mass of nanoparticle to the interface is denoted by $h\hat{z}$. The H_V and H_F are the half heights of octahedral silver nanoparticle in vertex up and facet up orientations, respectively.

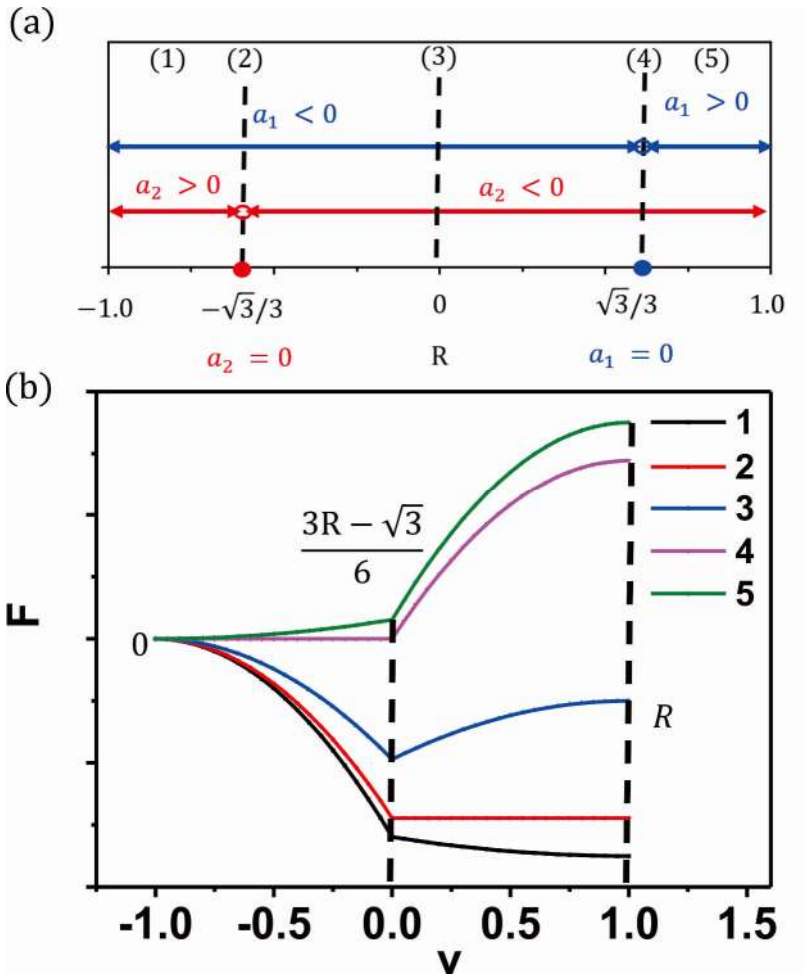

Figure 2. Sketch of the normalized free energy change F for vertex up orientation as a function of height ratio $v = h_V/H_V$. (a) The illustration of five regions based on the sign of a_1, and a_2. (b) In the five regions, the F curves depend on v and R. The curve 1, 2, 3, 4, and 5 are calculated when $R = -0.7$, $-\sqrt{3}/3$, -0.2, $\sqrt{3}/3$, and 0.7, which are in the region of $-1 \leq R < -\sqrt{3}/3$, $R = -\sqrt{3}/3$, $-\sqrt{3}/3 < R < \sqrt{3}/3$, $R = \sqrt{3}/3$ and $\sqrt{3}/3 < R \leq 1$, respectively.

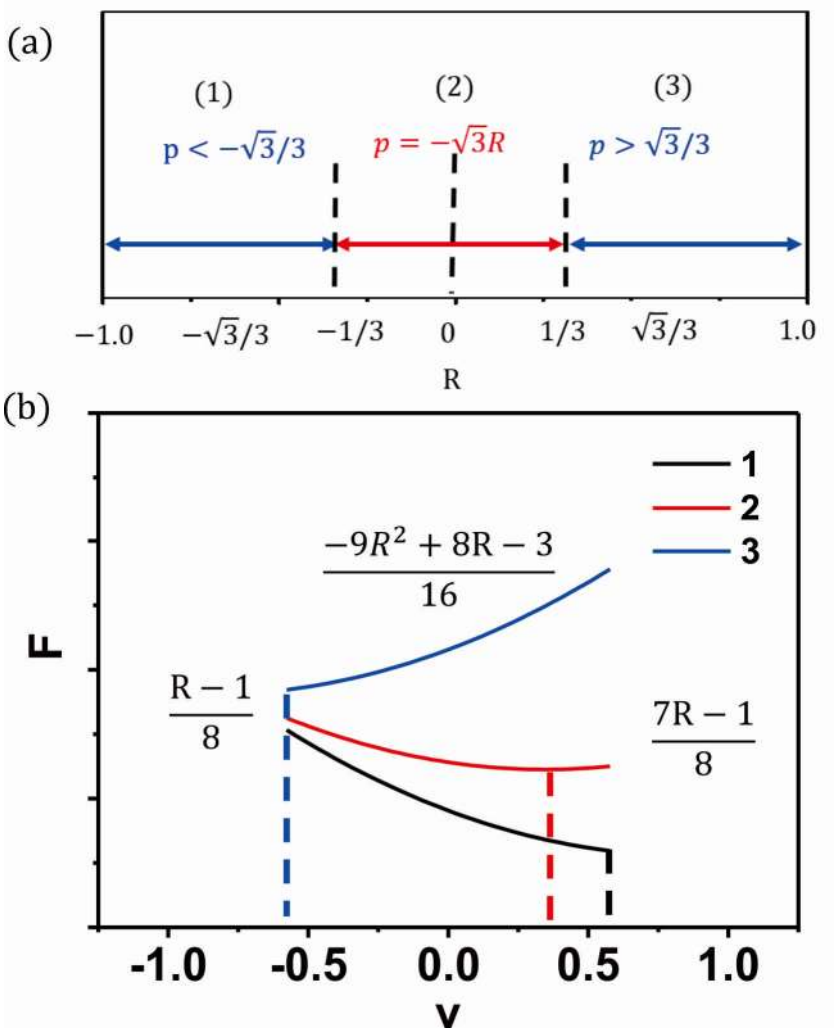

Figure 3. Sketch of the normalized free energy change F for facet up orientation as a function of relative height ratio $v = h_F/H_V$. (a) The illustration of three regions based on the position of symmetric axis p. (b) In the three regions, the F curves depend on v and R. The curve 1, 2 and 3 are calculated when $R = -0.5, -0.2$, and 0.5, which are in the region of $-1 \leq R < -1/3$, $-1/3 \leq R \leq 1/3$, and $1/3 < R \leq 1$, respectively.

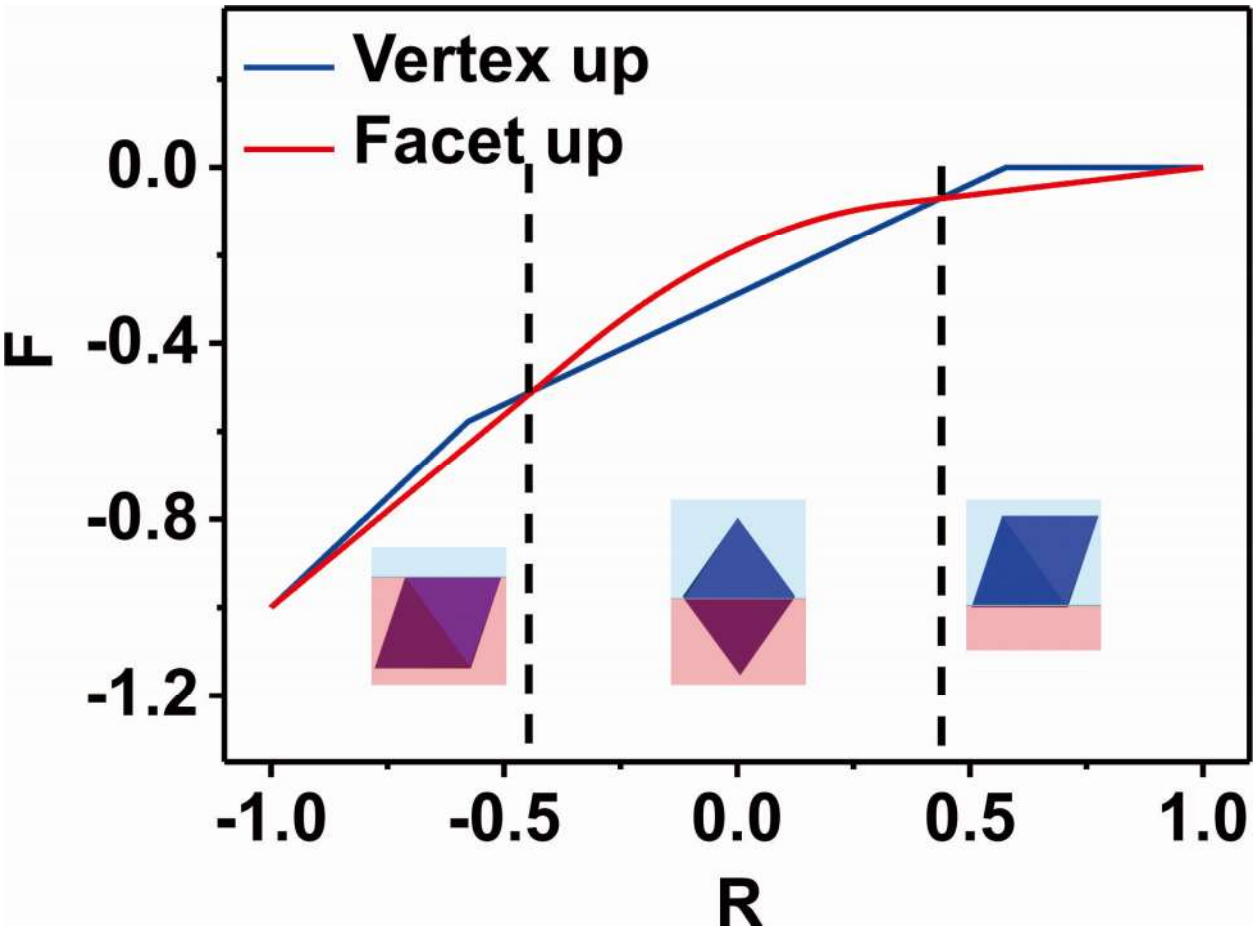

Figure 4. Dependence of the minimum of free energy change F on R for vertex up and facet up orientations. The values of R are $(3-4\sqrt{3})/9$ and $(4\sqrt{3}-3)/9$ for two vertical lines from left to the right, respectively.

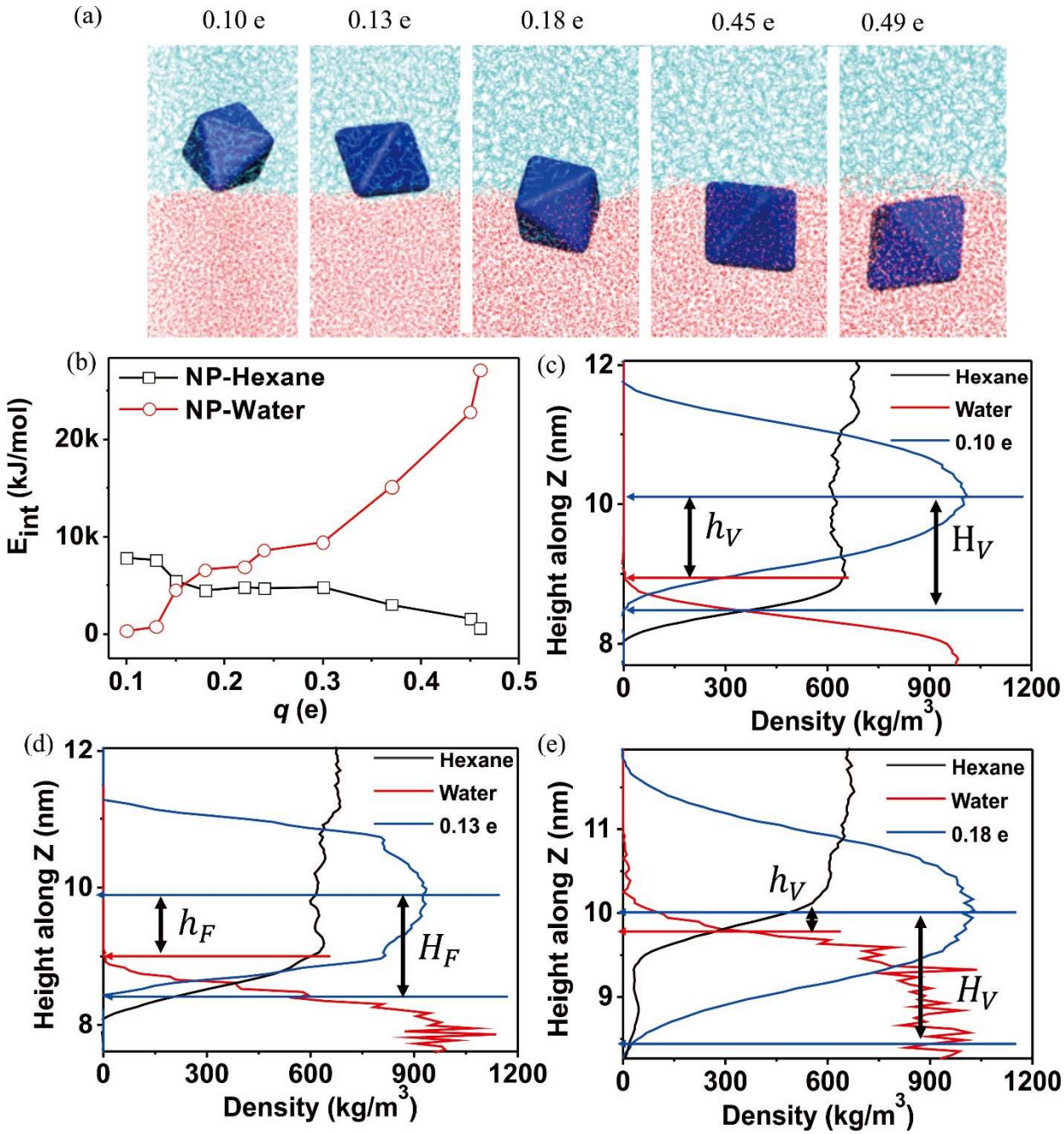

Figure 5. a) Positions and orientations of Ag octahedrons at the vicinity of the water/hexane interface. The point charges (positive or negative) are distributed on Ag octahedral surface randomly, where the amount of charge at each point (q) is 0.10 e, 0.13 e, 0.18 e, 0.45 e, and 0.49 e, respectively. b) The interaction energy between one Ag octahedral nanoparticle and hexane (NP-Hexane) and that between one Ag octahedron and water (NP-Water) with different q. c) The calculation of v and H_V using density distribution of one Ag octahedron system with q = 0.10 e. The v depends on the relative position of octahedron to the position of oil/water interface. The position of interface is defined as the starting point of density curve of

the water phase near the surface. The value of H_V is the half of the total octahedron height when the octahedron is close to a vertex up orientation. d) The position of interface is defined as the starting point of density curve of the water phase near the surface for q = 0.13 e. The value of HF is the half of the total octahedron height when the octahedron is close to a facet up orientation. e) The position of interface is defined as middle line of two solvent density curves near the surface for q = 0.18 e. The value of H_V is the half of the total octahedron height when the octahedron is close to a vertex up orientation.

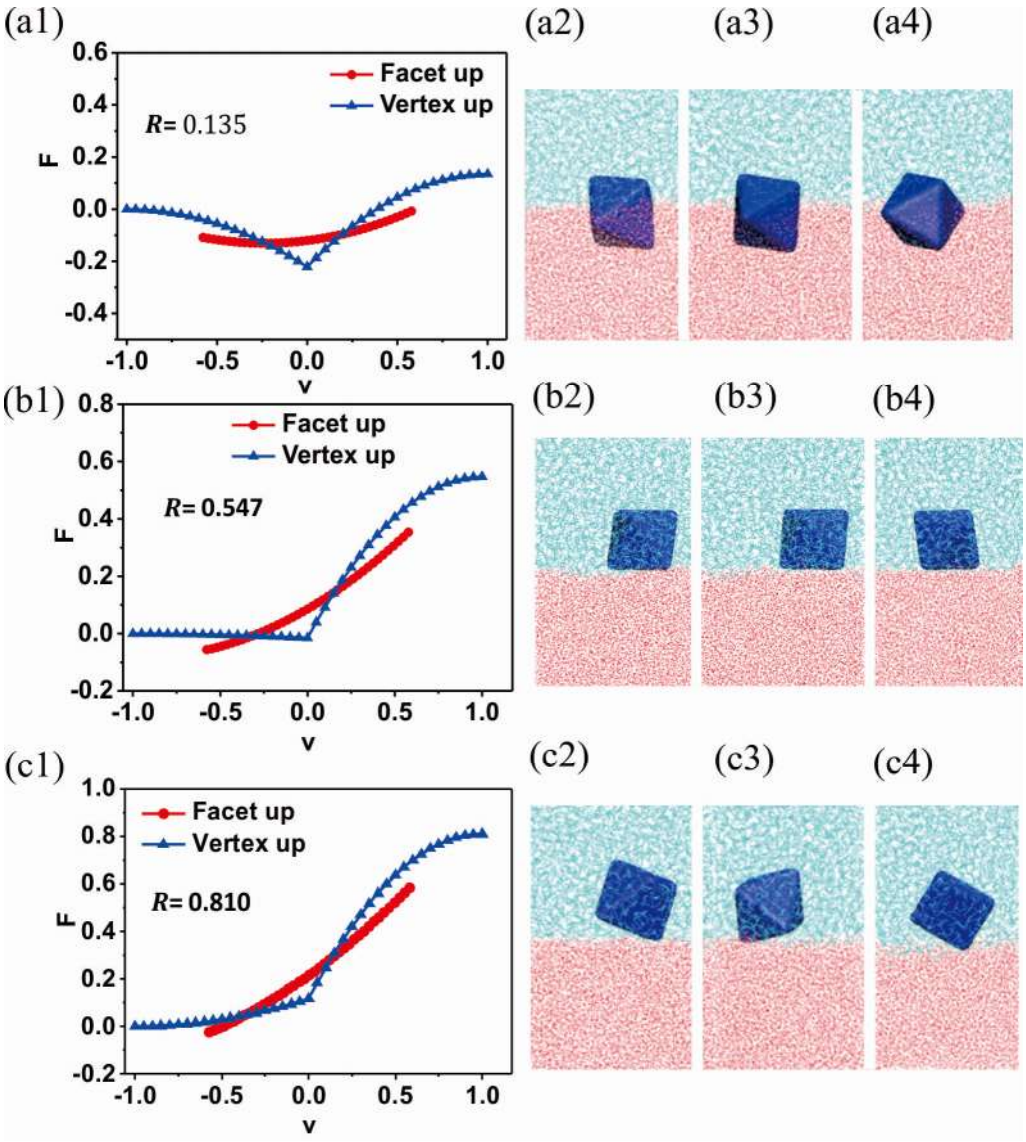

Figure 6. Free energy change curve (a1, b1, and c1) and snapshots (a2-a4, b2-b4, c2-c4) of molecular dynamics simulations with different R at the vicinity of the hexane/water interface. The octahedral Ag nanoparticles with different value of q: (a1-a4) 0.18 e, (b1-b4) 0.13 e, and (c1-c4) 0.10 e. The time interval for snapshots is roughly 200 ps. The free energy change is normalized by $A\gamma_{wo}$, which equals 348.7 k_BT.

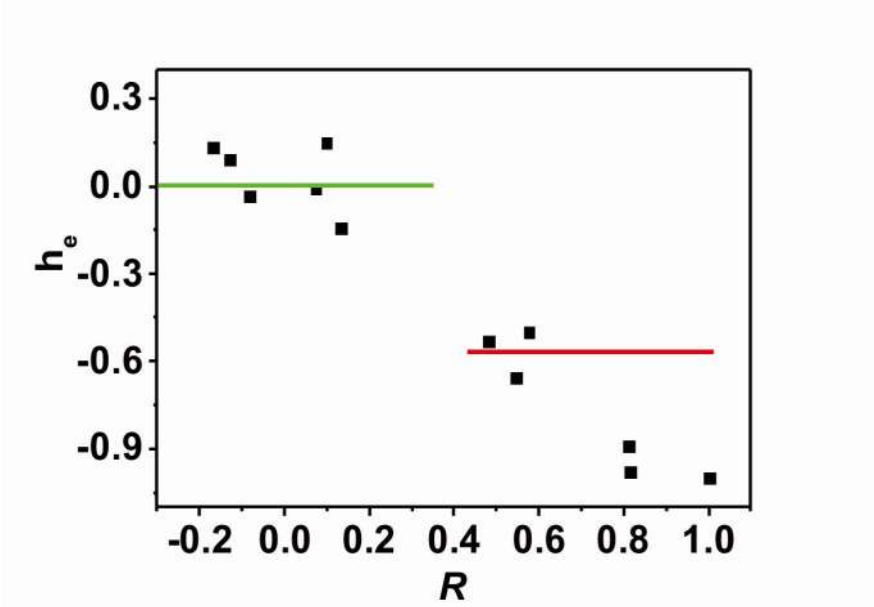

Figure 7. The relationship between the equilibrium height ratio h_e (h_e equals the v with the lowest free energy) and surface tension ratio R for octahedral Ag nanoparticle. The green straight lines $h_e = 0$ in the regions of $(3 - 4\sqrt{3})/9 \leq R \leq (4\sqrt{3} - 3)/9$, and the red straight line with $h_e = -\sqrt{3}/3$ in the region of $(4\sqrt{3} - 3)/9 < R \leq 1$, are from free energy change theory prediction, respectively.

Table 1. The analytic solution for the minimum of free energy change F for vertex up orientation.

	Region	a_1	a_2	$-b_1/2a_1$	$-b_2/2a_2$	The minimum of F	The minimum position h_e
1	$-1 \le R < -\sqrt{3}/3$	< 0	> 0	-1	1	R	$h_e^N = 1$,
2	$R = -\sqrt{3}/3$	< 0	$= 0$	-1	\	R	/
3	$-\sqrt{3}/3 < R < \sqrt{3}/3$	< 0	< 0	-1	1	$(3R - \sqrt{3})/6$	$h_e^N = 0$
4	$R = \sqrt{3}/3$	$= 0$	< 0	\	1	0	/
5	$\sqrt{3}/3 < R \le 1$	> 0	< 0	-1	1	0	$h_e^N = -1$

Table 2. The analytic solution for the minimum of free energy change F for facet up orientation.

	Region	The minimum of F	h_e
1	$-1 \le R < -1/3$	$(7R - 1)/8$	$\sqrt{3}/3$
2	$-1/3 \le R \le 1/3$	$(-9R^2 + 8R - 3)/16$	$-\sqrt{3}R$
3	$1/3 < R \le 1$	$(R - 1)/8$	$-\sqrt{3}/3$

Table 3. The analytic solution for the minimum of free energy change F for vertex up and facet up orientations.

	Region	Vertex up	Facet up	Preferred Orientation	h_e
1	$-1 \le R < (3 - 4\sqrt{3})/9$	R	$(7R - 1)/8$	Facet up	$\sqrt{3}/3$, in water
2	$(3 - 4\sqrt{3})/9 \le R \le (4\sqrt{3} - 3)/9$	$(3R - \sqrt{3})/6$	$(-9R^2 + 8R - 3)/16$	Vertex up	0, half oil, half water
3	$(4\sqrt{3} - 3)/9 < R \le 1$	0	$(R - 1)/8$	Facet up	$-\sqrt{3}/3$, in oil

Table 4. The preferred orientation from MD simulation for Ag Octahedron with different q.

q(e)	$\cos\theta$	R	Region	MD: h_e	MD: Orientation
0.1	-0.810 ± 0.037	0.810 ± 0.037	$(4\sqrt{3} - 3)/9 < R \le 1$	-0.891	Vertex up
0.13	-0.547 ± 0.021	0.547 ± 0.021	$(4\sqrt{3} - 3)/9 < R \le 1$	-0.660	Facet up
0.18	-0.135 ± 0.043	0.135 ± 0.043	$(3 - 4\sqrt{3})/9 \le R \le (4\sqrt{3} - 3)/9$	-0.141	Vertex up

TOC

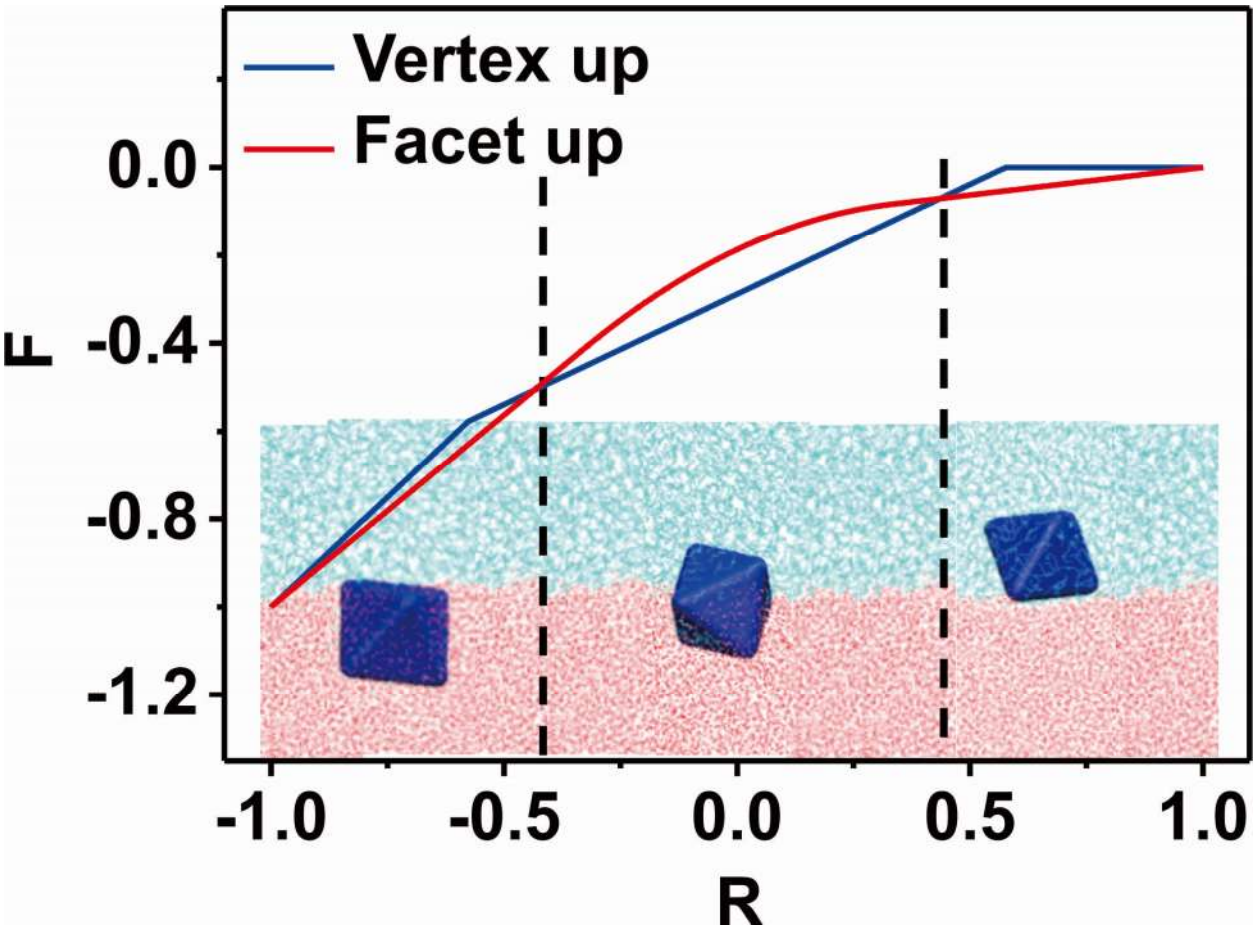

The agreement of molecular dynamics simulations results and our theoretical prediction of Ag octahedral nanoparticle at a hexane/water interface.